Supplementary Information

Defect Inducing Large Spin Orbital Coupling Enhances Magnetic Recovery Dynamics in CrI_3 Monolayer

Yu Zhou,[1] Ke Zhao,[1*] Zhenfa Zheng,[2] Huiwen Xiang,[1] Jin Zhao,[2*] Chengyan Liu[1*]

[1]Henan Key Laboratory of Quantum Materials and Quantum Energy, School of Quantum Information Future Technology, Henan University, Kaifeng, Henan 475001, China

[2]ICQD/Hefei National Laboratory for Physical Sciences at Microscale, and CAS Key Laboratory of Strongly-Coupled Quantum Matter Physics, and Department of Physics, University of Science and Technology of China, Hefei, Anhui 230026, China

E-mail: zhaoke312@126.com; cyliu@henu.edu.cn; zhaojin@ustc.edu.cn

Part I. Nonadiabatic Molecular Dynamics Theory

The spin dynamics are simulated using the home-made Hefei-NAMD code, which integrates the fewest-switches surface hopping (FSSH)[1] method with time-dependent density functional theory (TDDFT)[2]. The nuclear degrees of freedom are treated classically within the classical-path approximation (CPA)[2], where they remain uncoupled from the dynamics of the electron subsystem. The electronic Hamiltonian is parametrically dependent on the classical nuclear coordinates, which evolve along an *ab initio* molecular dynamics (AIMD) trajectory. Therefore, the time-dependent Schrödinger equation (TDSE) of electronic states incorporating spin-orbital coupling (SOC) can be formulated as:

$$i\hbar\frac{\partial}{\partial t}\left|\Phi(\mathrm{r},\mathrm{R},\sigma)\right\rangle = \hat{H}(\mathrm{r},\mathrm{R},\sigma)\left|\Phi(\mathrm{r},\mathrm{R},\sigma)\right\rangle \tag{S1}$$

where σ denotes the spin index, and the total Hamiltonian consists of a spin-free term and a SOC term

$$\hat{H}^{\mathrm{tot}}(\mathrm{r},\mathrm{R},\sigma) = \hat{H}_0(\mathrm{r},\mathrm{R}(t)) + \hat{H}^{\mathrm{SOC}}(\mathrm{r},\mathrm{R}(t)) \tag{S2}$$

The wave function can be expanded using Kohn-Sham (KS) orbitals $\left\{\left|\psi_i(\mathrm{r};\mathrm{R}(t))\right\rangle\right\}$ as a basis set,

$$\left|\Phi(\mathrm{r},\mathrm{R},\sigma)\right\rangle = \sum_i \left|\psi_i\right\rangle\left\langle\psi_i\middle|\Phi(\mathrm{r},\mathrm{R},\sigma)\right\rangle = \sum_i c_i\left|\psi_i\right\rangle \tag{S3}$$

Substituting Eq. (S3) into Eq. (S1) yields the equation governing the expansion coefficients

$$\begin{aligned} i\hbar\frac{\partial c_i(t)}{\partial t} &= \sum_j \left[\left\langle\psi_i\middle|\hat{H}^{\mathrm{tot}}\middle|\psi_j\right\rangle - i\hbar\left\langle\psi_i\middle|\frac{\mathrm{d}}{\mathrm{d}t}\middle|\psi_j\right\rangle\right] c_j(t) \\ &= \sum_j \left[\left\langle\psi_i\middle|\hat{H}_0\middle|\psi_j\right\rangle + \left\langle\psi_i\middle|\hat{H}^{\mathrm{soc}}\middle|\psi_j\right\rangle - i\hbar\left\langle\psi_i\middle|\frac{\mathrm{d}}{\mathrm{d}t}\middle|\psi_j\right\rangle\right] c_j(t) \\ &= \sum_j \left[H_{ij}^0 + H_{ij}^{\mathrm{SOC}} - i\hbar T_{ij}\right] c_j(t) \end{aligned} \tag{S4}$$

where $T_{ij} = \langle \psi_i | \frac{\mathrm{d}}{\mathrm{d}t} | \psi_j \rangle$ can be transformed to $\dot{\mathrm{R}} \cdot (\varepsilon_j - \varepsilon_i)^{-1} \cdot \langle \psi_i | \nabla_{\mathrm{R}} \hat{H} | \psi_j \rangle$ and this term is contributed by electron-phonon coupling (EPC). For nonadiabatic molecular dynamics (NAMD) without SOC, the nonadiabatic coupling (NAC) term governs the transition probability between KS orbitals. In addition to the EPC, the SOC contribution is incorporated into the NAC. The spin-orbital Hamiltonian is given by

$$\hat{H}^{\mathrm{SOC}} = \frac{\hbar \sigma \cdot \mathrm{p} \times \nabla v_{\mathrm{KS}}(\mathrm{r})}{4m^2c^2} \tag{S5}$$

Where $v_{\mathrm{KS}}(\mathrm{r})$ is the spin-dependent part of the KS potential. Due to the derivative of the KS potential in Eq. (S5), the SOC is dominated by the regions close to the nuclei. In the projector augmented wave (PAW) formalism, the all-electron orbitals in these regions can be expanded as

$$\psi_i = \sum_k \langle \widetilde{p}_k | \widetilde{\psi}_i \rangle | \widetilde{\phi}_k \rangle \tag{S6}$$

where $\widetilde{p}_k$ and $\widetilde{\phi}_k$ are the projector function and all-electron partial waves, respectively. Then, the SOC matrix elements become

$$H_{ij}^{\mathrm{SOC}} = \sum_{kl} \langle \widetilde{\psi}_i | \widetilde{p}_k \rangle \langle \phi_k | \widetilde{H}^{\mathrm{SOC}} | \phi_l \rangle \langle \widetilde{p}_l | \widetilde{\psi}_j \rangle \tag{S7}$$

where the matrix elements in the right-hand side of Eq. (S7) are calculated by VASP.

In the NAMD simulations, two types of basis sets are used in Eq. (S3). One is the spin-polarized KS orbitals, which are themselves eigenfunctions of $\widetilde{H}_0$ and shall be referred to as the spin-diabatic representation. In this case, the matrix elements not only include the EPC term (T_{ij}) but also the SOC term (H_{ij}^{SOC}). While the nonradiative relaxation between the states with the same spin is determined by T_{ij}, the spin-flip probability is decided by H_{ij}^{SOC}. These two different contributions can be distinguished clearly. On the other hand, we can also diagonalize the Hamiltonian in Eq. (S4) to get the spinor basis sets for the time propagation, which is referred to as the spin-adiabatic representation. The two-component spinor wave function can be written as

$$| \phi_k \rangle = \begin{pmatrix} | \psi_i^{\uparrow} \rangle \\ | \psi_i^{\downarrow} \rangle \end{pmatrix} \tag{S8}$$

In this case, the NAC between different spinor states can be expressed as

$$T_{ij} = \langle \psi_i | \frac{\mathrm{d}}{\mathrm{d}t} | \psi_j \rangle = \left(\langle \psi_i^{\uparrow} |, \langle \psi_i^{\downarrow} | \right) \frac{\mathrm{d}}{\mathrm{d}t} \begin{pmatrix} | \psi_i^{\uparrow} \rangle \\ | \psi_i^{\downarrow} \rangle \end{pmatrix} \tag{S9}$$

In the spin-adiabatic representation, both the EPC and SOC effects are mixed together

in the NAC elements[3].

Part II. Surface hopping, fewest surface hopping and spin flux

A. Surface hopping

Assuming that the splitting of the nuclear wave packet after passing through the nonadiabatic coupling region can be modeled as a set of mutually independent trajectories, where each trajectory evolves on a single potential energy surface at any given time, the hopping of carriers between trajectories is referred to as the surface hopping method.

The equation of motion for the nucleus is given by

$$M_a \ddot{R}_a^I = -\nabla_a E_k^{el}(R^l) \tag{S10}$$

where I denotes the Ith trajectory. The electronic wave function is then expanded in a set of orthonormal basis functions as

$$\Phi^I(r,R,t) = \sum_i^{\infty} C_j^I(t)\phi_j^I(r,R) \tag{S11}$$

Substituting equation (S11) into the time-dependent Schrödinger equation yields

$$\dot{C}_j^I(t) = -\frac{i}{\hbar} C_j^I(t) E_j^I - \sum_k C_k^I(t)\dot{R}^I \cdot d_{jk}^I(R) \tag{S12}$$

The expansion coefficients can further be expressed in an exponential form $C_j^I = \widetilde{C}_j^I \exp[-\frac{i}{\hbar}\int_0^t E_j^I d\tau]$. Rewriting equation (S12) in the form of a density matrix gives

$$\dot{\rho}_{jk}^I = -\frac{1}{i\hbar}\rho_{jk}^I(E_k - E_j) - \sum_l (\rho_{jl}^I d_{kl}^I - \rho_{lk}^I d_{lj}^I)\cdot \dot{R}^I \tag{S13}$$

where $\rho_{jk}(t) = C_j^*(t)C_k(t)$ and the trace is

$$\dot{\rho}_{jj}^I = \sum_{k\neq j} -2\,\mathrm{Re}[\rho_{jk}^I d_{jk}^I \cdot \dot{R}^I] \tag{S14}$$

For a trajectory to hop between different potential energy surfaces, it must satisfy the condition of $N_j \propto \rho_{jj}$, ensuring that the number of trajectories on the jth electronic state is proportional to ρ_{jj}. This requirement is known as the "internal consistency" condition of the surface hopping method[4]. The fewest surface hopping method introduced below adheres to this condition.

B. Fewest surface hopping

Assuming there are N mutually independent nuclear trajectories, where N is sufficiently large and approaches infinity, and all trajectories share the same initial conditions, at time t, N_j trajectories reside on the potential energy surface corresponding to the jth electron state ϕ_j,

$$N_j(t) = \rho_{jj}(t)N; \qquad \sum_j N_j(t) = N \tag{S15}$$

At time $t' = t + \Delta t$, the number of trajectories on the *j*th electronic state changes to

$$N_j(t') = \rho_{jj}(t')N \tag{S16}$$

Assuming $\Delta N_j = N_j(t) - N_j(t') > 0$, while the fewest surface hopping, which accounts for the reduction in occupation number, allows trajectories to hop out of state *j* but does not permit transitions from other states into state *j*.

Hence, the probability $P_j(t, \Delta t)$ of the system transitioning from state *j* to other states over time $[t, t + \Delta t]$ is given by

$$P_j(t, \Delta t) = \frac{\Delta N_j}{N} = \frac{\rho_{jj}(t) - \rho_{jj}(t')}{\rho_{jj}} \approx -\frac{\dot{\rho}_{jj}(t)\Delta t}{\rho_{jj}} \tag{S17}$$

Substituting equation (S14) into equation (S17) yields:

$$\mathrm{P}_j(t, \Delta t) = \frac{2\mathrm{Re}\left[\rho_{\mathrm{jk}} d_{jk} \cdot \dot{R}\right]\Delta t}{\rho_{jj}} \tag{S18}$$

The sum of the transition probabilities from state *j* to other states $k \neq j$ represents the total probability of the system hopping out of the state *j*:

$$P_j(t, \Delta t) = \sum_{k \neq j} P_{j \to k}(t, \Delta t) \tag{S19}$$

Assuming that the transition processes from state *j* to state *k* are mutually independent, we obtain

$$P_{j \to k}(t, \Delta t) = \frac{2\mathrm{Re}[\rho_{jk} d_{jk} \cdot \dot{R}]\Delta t}{\rho_{jj}} \tag{S20}$$

The above derivation is based on the assumption that the occupation number of state *j* decreases. However, in fact, there are cases where the occupation number of state *j* increases. In such instances, trajectories do not hop out of the current electronic state, namely $P_{j \to k}(t, \Delta t) = 0$. Therefore, the reasonable trajectory hopping probability can be given by

$$\mathrm{G}_{j-k}(t, \Delta t) = \max[P_{j \to k}(t, \Delta t), 0] \tag{S21}$$

The implementation of the minimal surface hopping algorithm is introduced below. A uniformly distributed random number ξ in the range [0,1) is generated. If the following condition is satisfied

$$\sum_{k=1, k \neq j}^{n-1} G_{j \to k} < \xi < \sum_{k=1, k \neq j}^{n} G_{j \to k} \tag{S22}$$

the trajectory hops from state *j* to state *n*. Conversely, no hopping occurs, and the trajectory remains in state *j*.

C. Definition of spin flux

At time t = 0, the number of occupations on the kth energy band during the mth hopping event is $Pop_{m0k}=1$, while $k'\neq k$, the number of occupations is $Pop_{m0k'}=0$.

In surface hopping simulations, based on the criterion given in equation (S22), each time an electron transitions from band i to band j at time t given by

$$Pop_{mti}=Pop_{mti}-1,\quad Pop_{mtj}=Pop_{mtj}+1 \tag{S23}$$

After N hopping attempts, the final fractional distribution of occupations is give by

$$pop_{tj}=\sum_{l=1}^{N}Pop_{mtj}/N \tag{S24}$$

For the spin flux of interest, each time a carrier transitions from state a to state b, the corresponding count of evens is given by

$$F_{mta\to b}=F_{mta\to b}+1 \tag{S25}$$

Subsequently, after N hopping attempts, the final spin flux from state a to state b is given by

$$f_{mta\to b}=\sum_{m=1}^{N}F_{mta\to b}/N \tag{S26}$$

Part III. Figures in supplementary materials

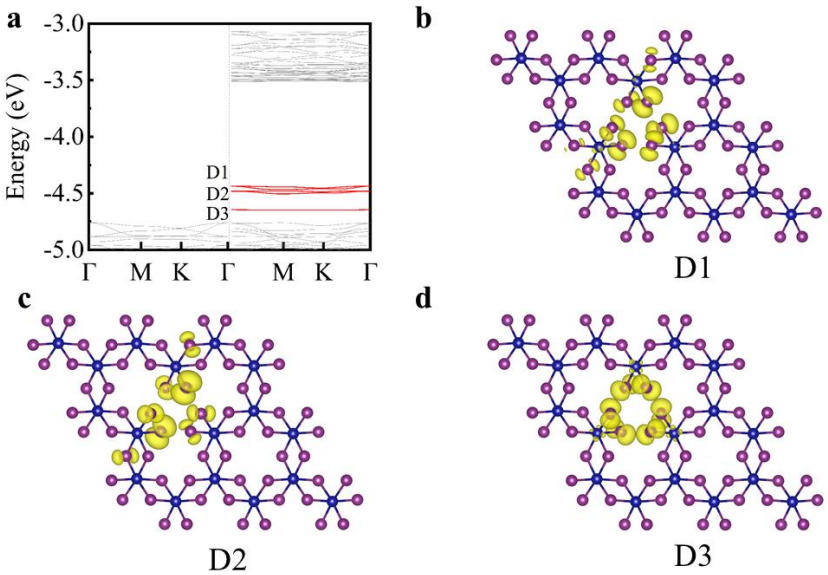

Supplementary Fig. S1 | Band structure and partial charge density of the V_{Cr} defect system. **a** Band structure. **b-d** Partial charge densities of the defect levels corresponding to D1, D2 and D3 labeled in **a**, respectively. D1 and D2 are doublets, and D3 is singlet at the Γ-point. The isovalue of isosurface charge density is 0.002 e/Å^3. Violet and blue balls represent I and Cr atoms, respectively.

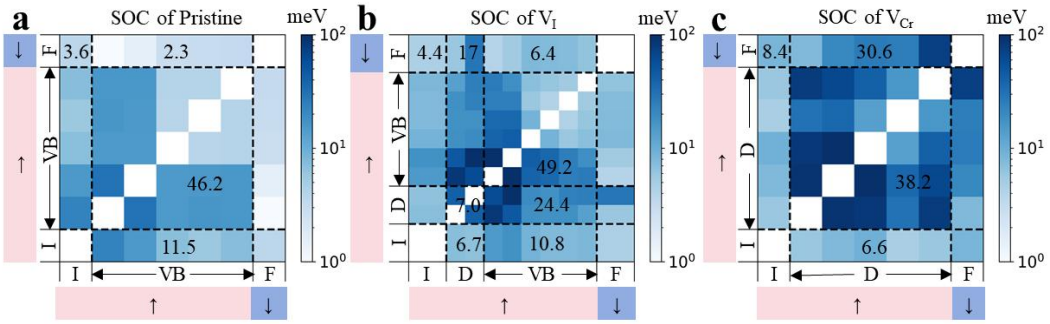

Supplementary Fig. S2 | 2D visualization of complete SOC data. a-c the pristine, V_I and V_{Cr} systems. Short arrows "↑" and "↓" denote spin-up and spin-down states, respectively. "I", "F" and "D" represent initial, final and defect states, respectively.

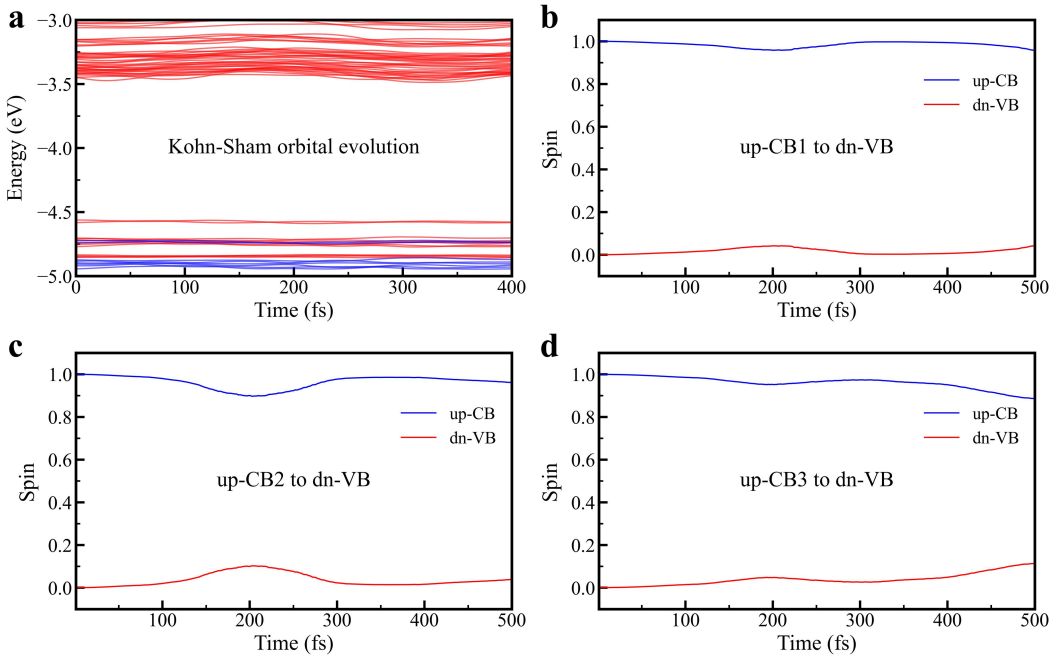

Supplementary Fig. S3 | Kohn-Sham orbital and population for the pristine system. a Kohn-Sham orbital evolution. **b-d** population evolution of an electron with initial states at up-CB1, up-CB2 and up-CB3, respectively, and a final state at dn-VB. The up-CB1, up-CB2 and up-CB3 correspond to the lowest, second-lowest and third-lowest spin-up conduction bands, respectively.

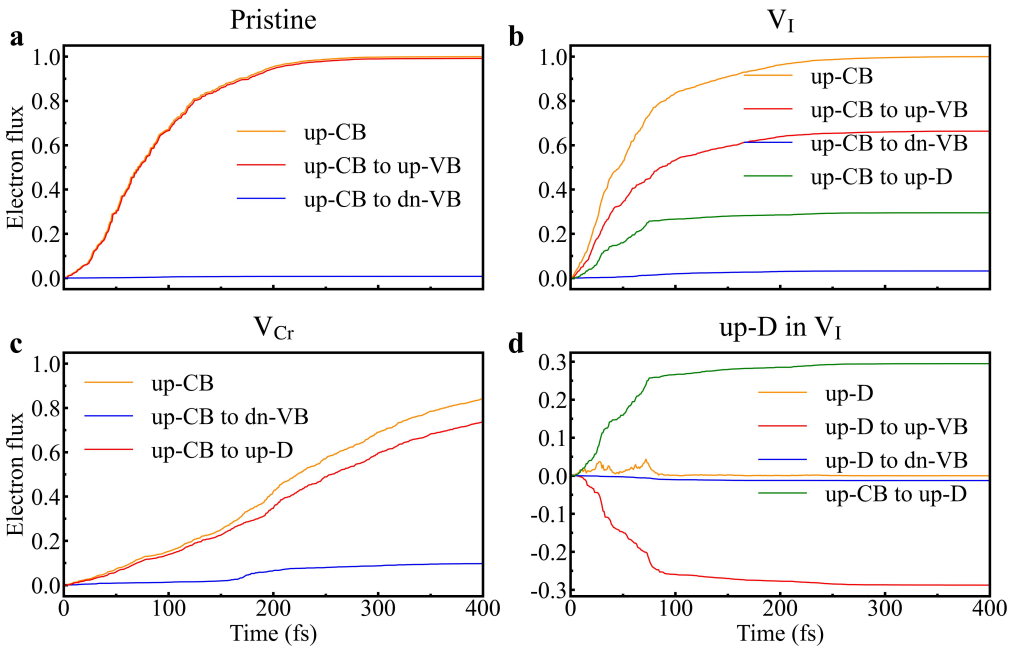

Supplementary Fig. S4 | Evolution of spin flux. a-c Evolution of the spin flux in up-CB states for the pristine, V_I and V_{Cr} systems, respectively. **d** Evolution of the spin flue in up-D states for the V_I systems. Positive values represent electron inflow, while negative values indicate outflow. In all three systems, the population flow from up-CB to dn-VB is negligible.

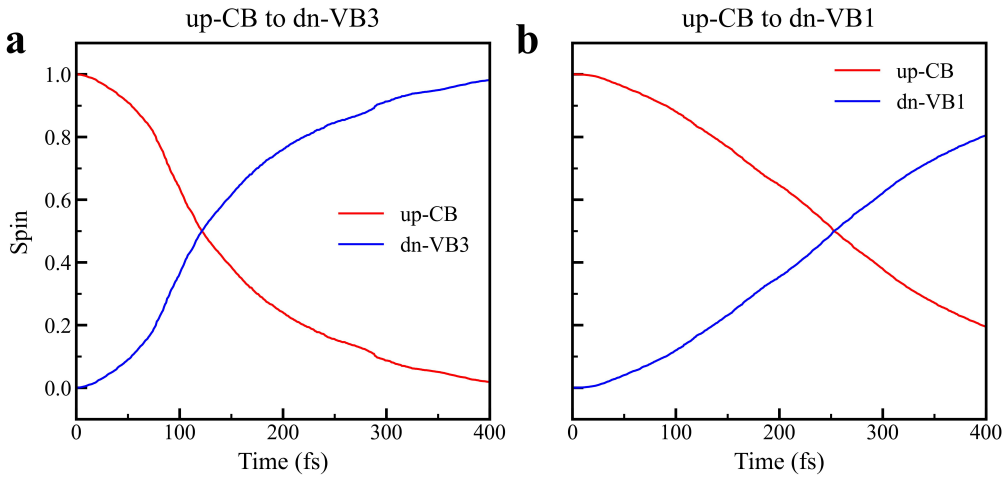

Supplementary Fig. S5 | Single-electron spin evolution of the V_{Cr} system under the different final-state conditions. a Electron transitions from the spin-up conduction band minimum to the third-highest spin-down valence band, with two higher-energy spin-up valence bands above it. **b** Electron transitions from the spin-up conduction band minimum to the spin-down valence band maximum, without any intermediate spin-up valence bands.

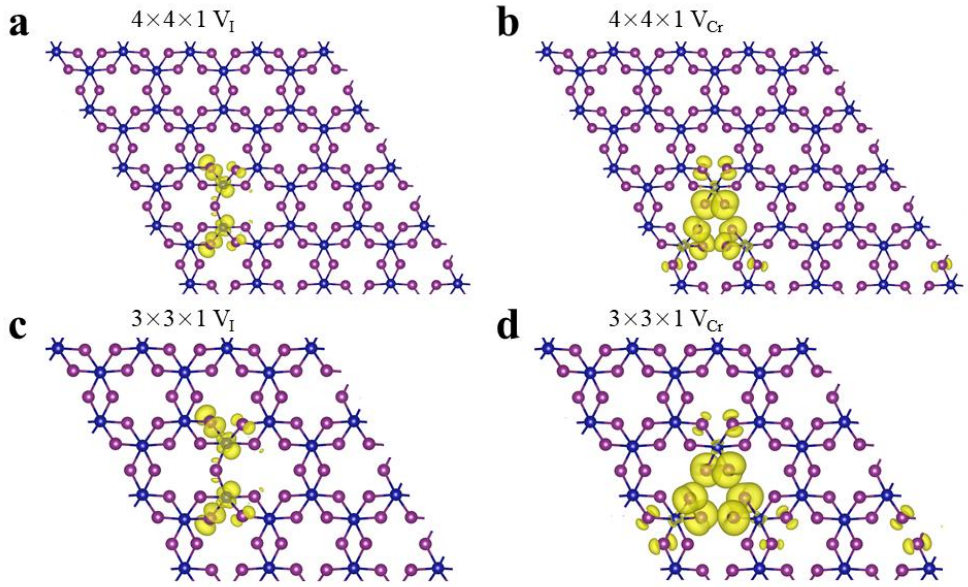

Supplementary Fig. S6 | Comparison of defect states in different supercells. a V_I in a 4 × 4 × 1 system. **b** V_{Cr} in a 4 × 4 × 1 system. **c** V_I in a 3 × 3 × 1 system. **d** V_{Cr} in a 3 × 3 × 1 system.

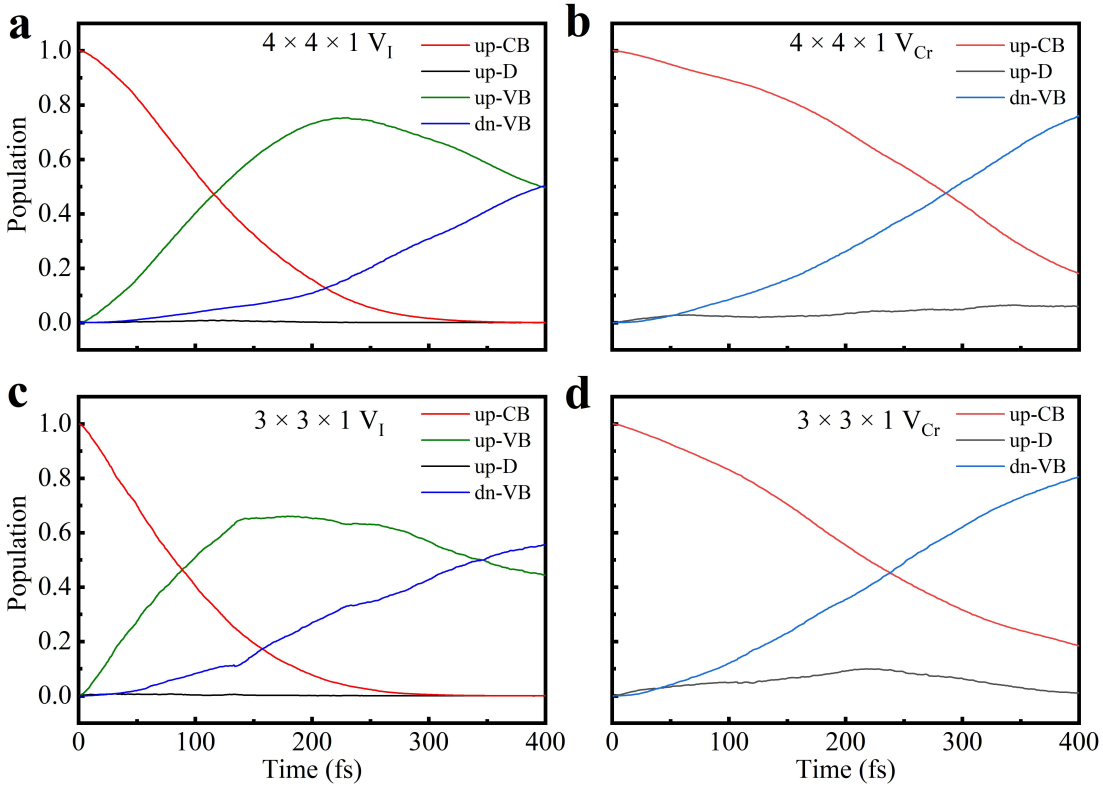

Supplementary Fig. S7 | Comparison of population evolution in different supercells. a V_I in a 4 × 4 × 1 system. **b** V_{Cr} in a 4 × 4 × 1 system. **c** V_I in a 3 × 3 × 1 system. **d** V_{Cr} in a 3 × 3 × 1 system.

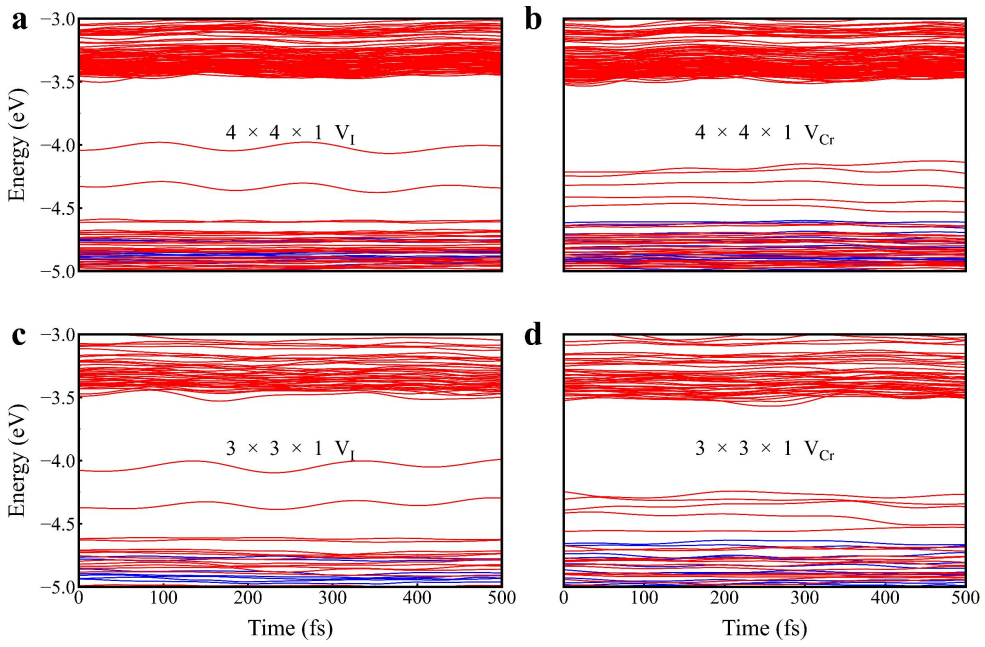

Supplementary Fig. S8 | Comparison of time-dependent Kohn-Sham orbital evolution in different supercells. a V_I in a 4 × 4 × 1 system. **b** V_{Cr} in a 4 × 4 × 1 system. **c** V_I in a 3 × 3 × 1 system. **d** V_{Cr} in a 3 × 3 × 1 system.

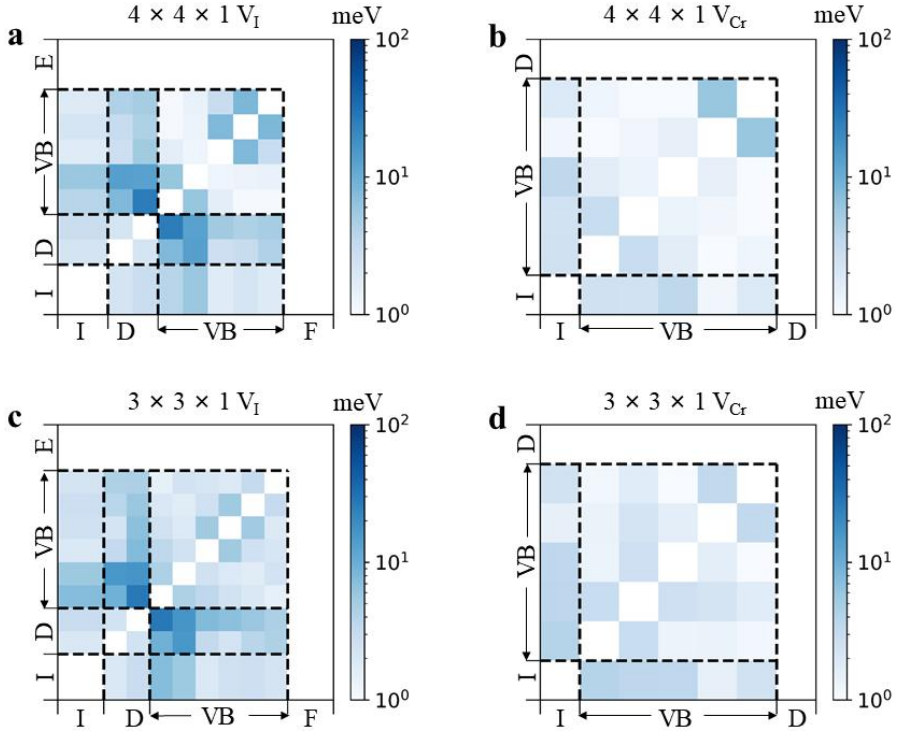

Supplementary Fig. S9 | Comparison of 2D visualization of EPC data in different supercells. a V_I in a 4 × 4 × 1 system. **b** V_{Cr} in a 4 × 4 × 1 system. **c** V_I in a 3 × 3 × 1 system. **d** V_{Cr} in a 3 × 3 × 1 system.

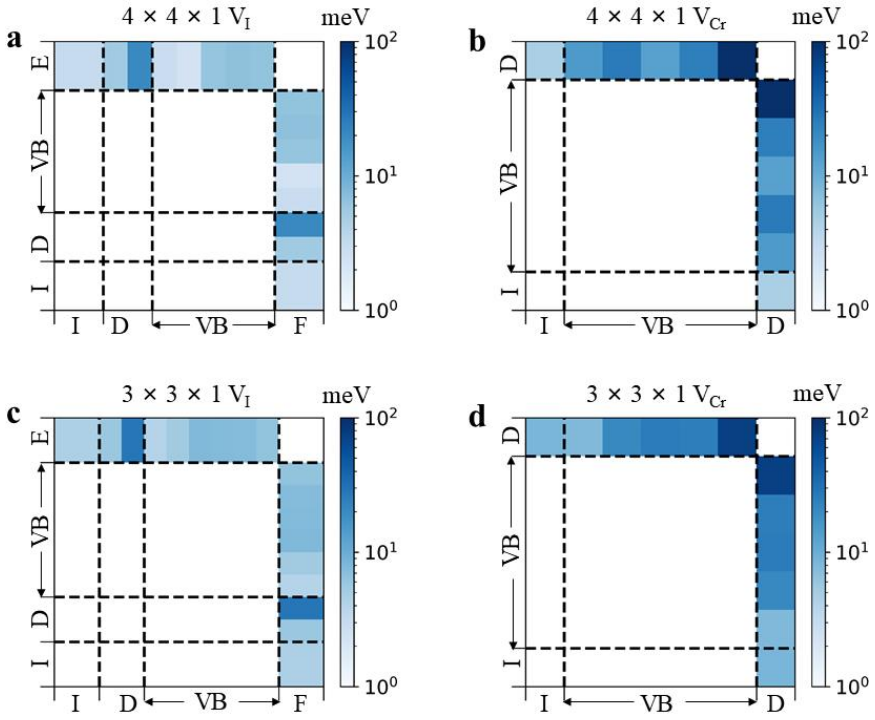

Supplementary Fig. S10 | Comparison of 2D visualization of SOC data in different supercells. **a** V_I in a 4 × 4 × 1 system. **b** V_{Cr} in a 4 × 4 × 1 system. **c** V_I in a 3 × 3 × 1 system. **d** V_{Cr} in a 3 × 3 × 1 system.

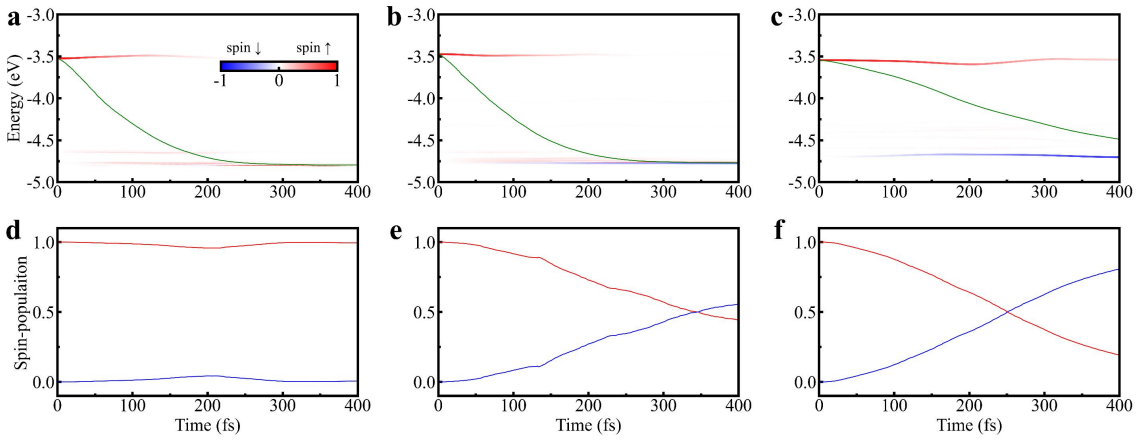

Supplementary Fig. S11 | Energy evolution and spin population over time. a-c Energy evolution of excited electron in the pristine, V_I and V_{Cr} systems, with the color map indicating orbital localization. **d-f** Spin relaxation of excited electron in the pristine, V_I and V_{Cr} systems.

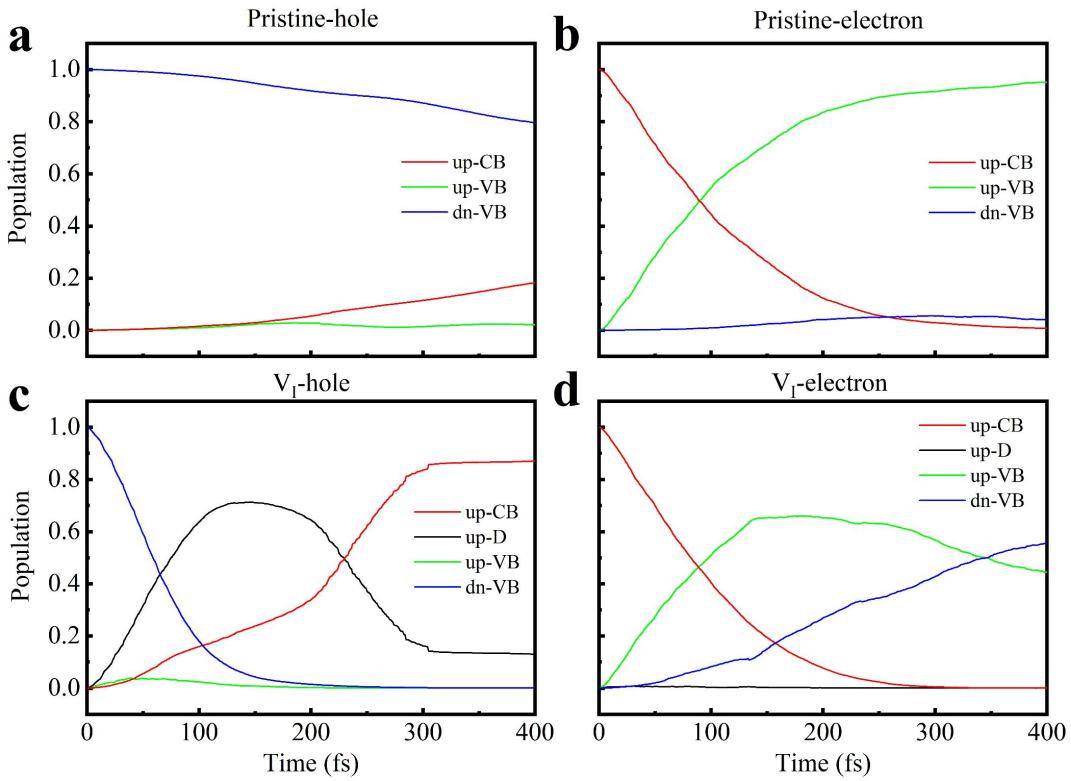

Supplementary Fig. S12 | Evolution of hole and electron spin fluxes. a, **c** Hole spin flux from the dn-VB to up-CB for pristine and V_I systems, respectively. **b**, **d** Electron spin flux from up-CB to dn-VB for pristine and V_I systems, respectively.

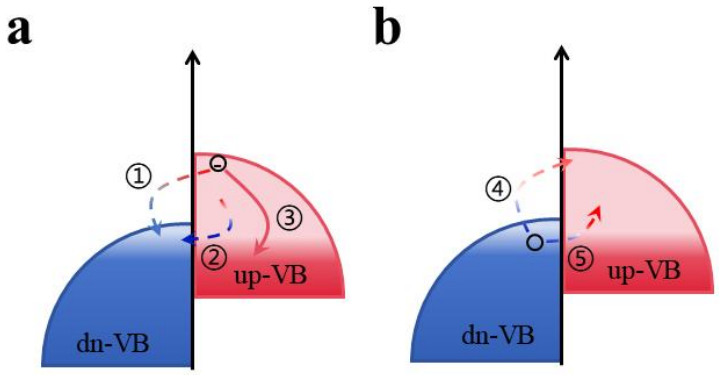

Supplementary Fig. S13 | Schematic illustration of single-electron/hole transition in the V_I system. a Single-electron transitions from up-spin VB to the down-spin VB. **b** Single-hole transitions from the down-spin VB to the up-spin VB.

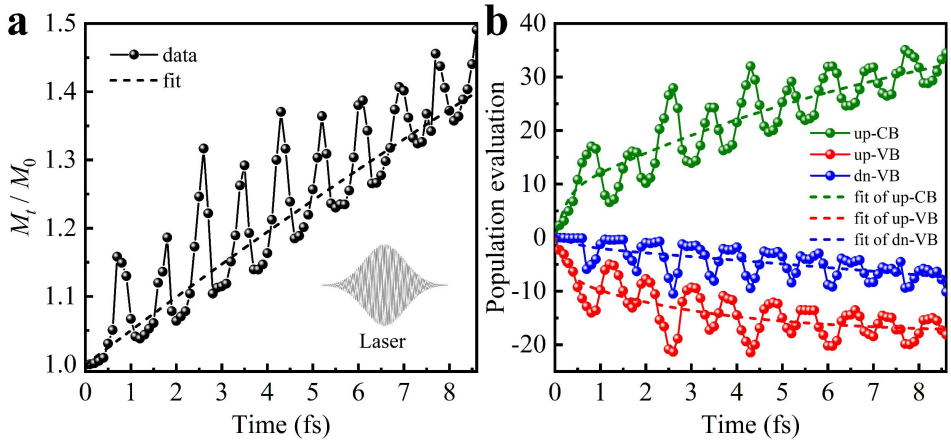

Supplementary Fig. S14 | Evolution process of pristine CrI_3 under laser pulse excitation. a Evolution of relative magnetic moment. The insert picture is the laser pulse signal shape. **b** Evolution of electronic population. M_0 and M_t are the magnetic moments of the systems in the unexcited state and at time t after excitation, respectively. Laser pulse initializes at 0 femtoseconds.

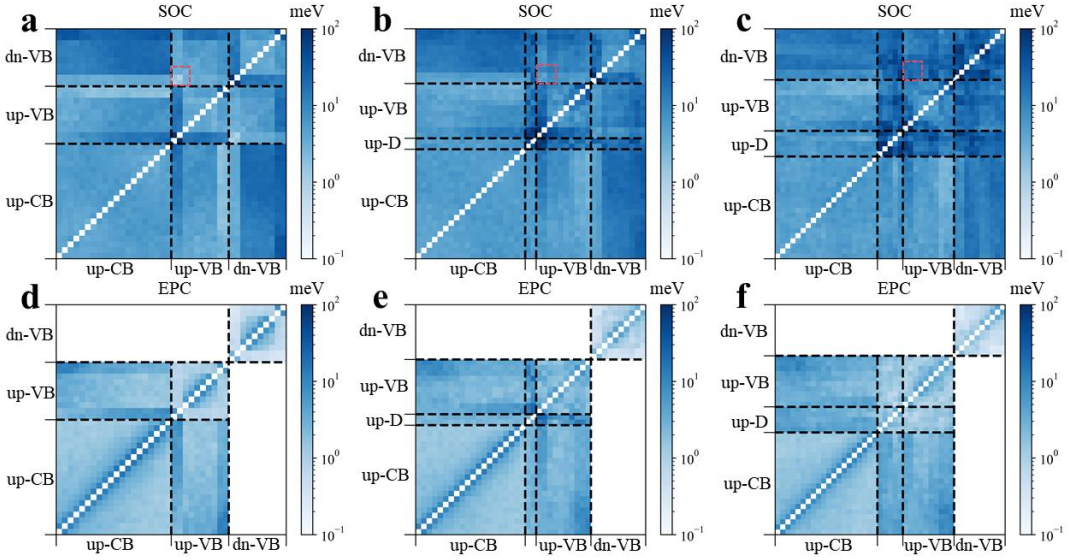

Supplementary Fig. S15 | 2D visualization of SOC and EPC in bands involved in multielectron spin relaxation dynamics. a-c SOC for the prototype, V_I and V_{Cr} systems. **d-f** EPC for the same systems. Red dashed box highlights the SOC between the upper regions of the up-VB and dn-VB states, with the corresponding SOC values of 1.22, 5.02, and 19.88 meV for the prototype, V_I and V_{Cr} systems, respectively.

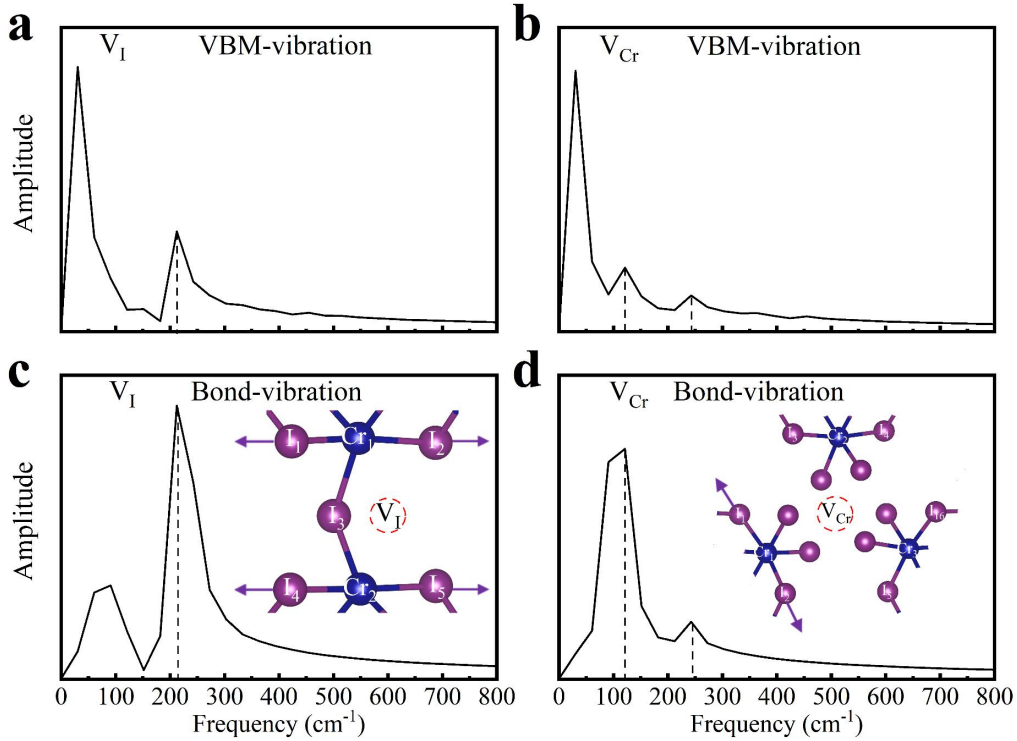

Supplementary Fig. S16 | Vibration spectra. Vibration spectra of VBM and chemical bond obtained by performing Fourier transform on the autocorrelation function of the fluctuations, based on 2000 ab initio molecular dynamic (AIMD) trajectories. **a**, **b** VBM vibration spectra of V_I and V_{Cr} systems. **c**, **d** Bond vibration spectra of V_I and V_{Cr} systems.

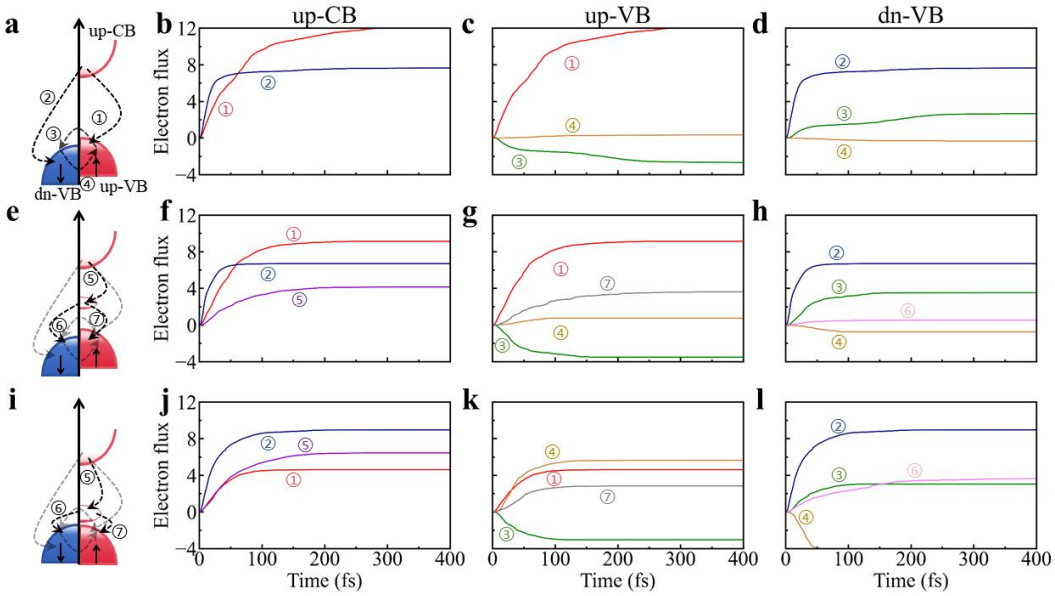

Supplementary Fig. S17 | Relaxation pathways of multielectron spin dynamics. a-d the pristine system. **e-h** the V_I system. **i-l** the V_{Cr} system. **a**, **e** and **i** Schematics of multielectron spin relaxation pathways. **b**, **f** and **j** Evolution of electron populations flowing from the up-CB reservoir to potential pathways in these three systems. **c**, **g** and **k** Evolution of electron populations in the up-VB reservoir, detailing both inflow and outflow pathways. **d**, **h** and **l** Evolution of

electron populations of the dn-VB reservoir, also detailing both inflow and outflow pathways. Processes ① to ⑦ correspond to specific spin relaxation pathways: process ①, up-CB to up-VB; process ②, up-CB to dn-VB; process ③, up-VB to dn-VB; process ④, dn-VB to up-VB; process ⑤, up-CB to up-D; process ⑥, up-D to dn-VB; and process ⑦, up-D to up-VB.

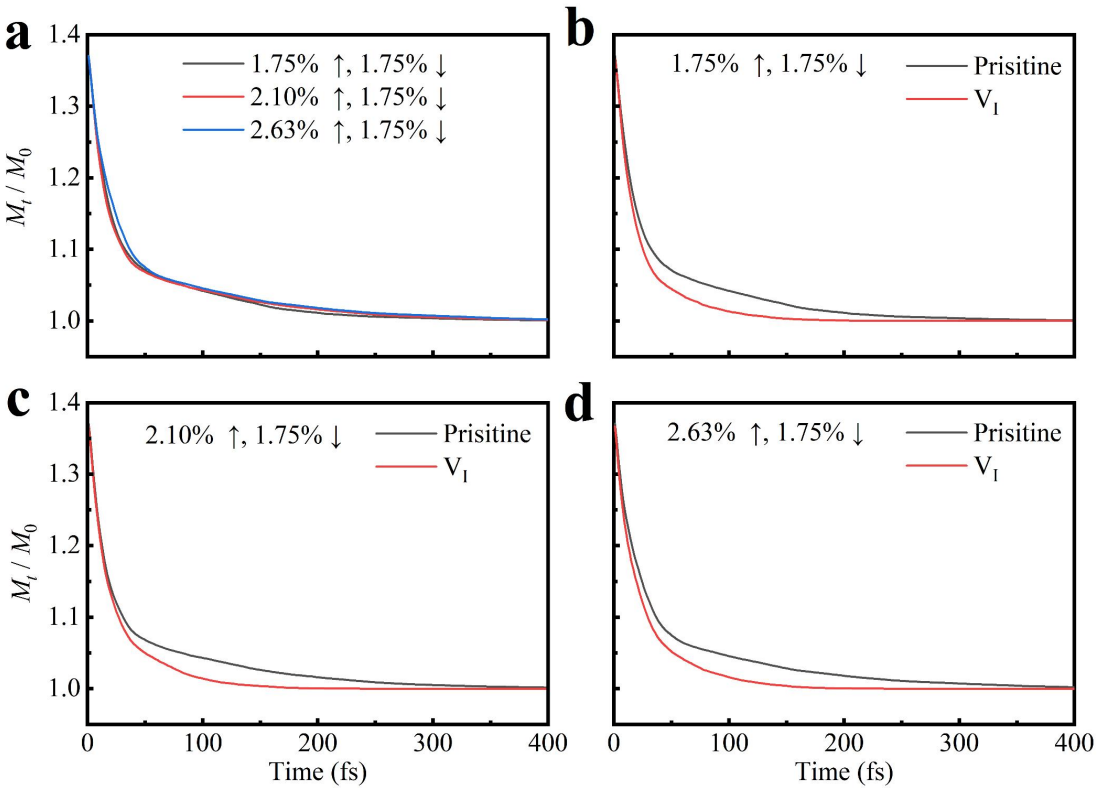

Supplementary Fig. S18 | Magnetic recovery rate at varying excited spin electron numbers. a In pristine system, the electronic excitation of spin-down remains at 1.75%, while the spin-up excitation is 1.75%, 2.10% and 2.63%, respectively, serving as the initial conditions for magnetic recovery processes. Magnetic recovery rates of pristine and VI systems are evaluated under initial condition of **b** 1.75% excited spin-up and 1.75% spin-down electrons, **c** 1.75% excited spin-up and 2.10% spin-down electrons, and **d** 1.75% excited spin-up and 2.63% spin-down electrons.

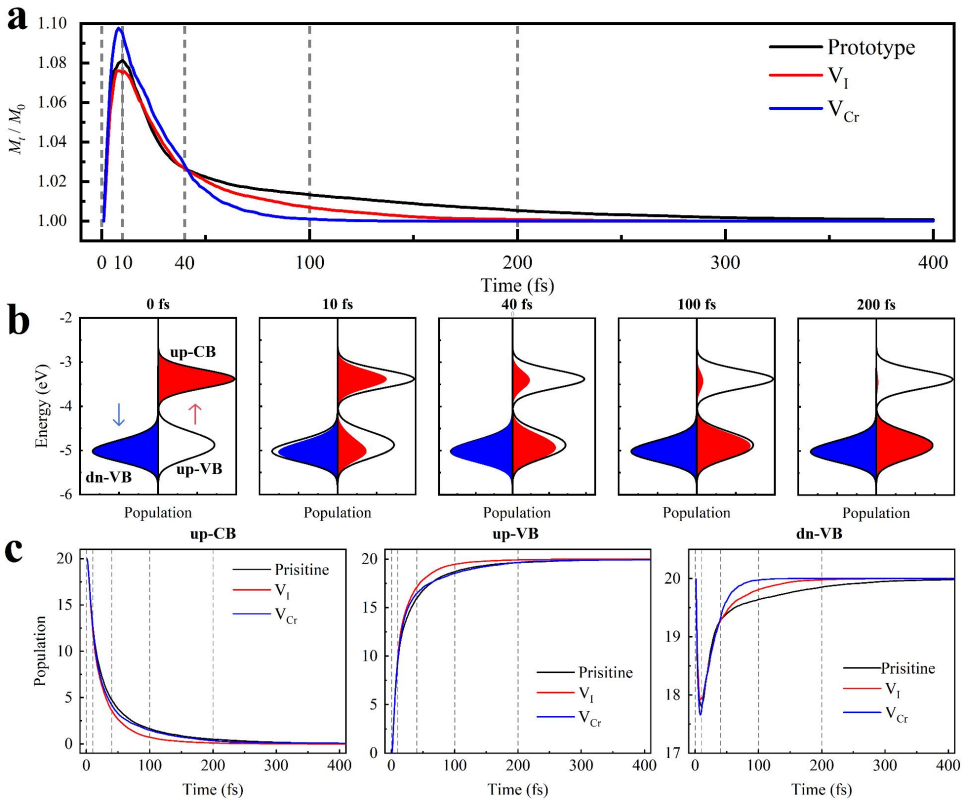

Supplementary Fig. S19 | Multielectron dynamics simulation where electrons excited to the up-CB states originate only from the up-VB states as the initial status. a Evolution of relative magnetic moments for these three systems. **b** Snapshots of the evolution of the occupied electron density of states in the prototype system. The black solid outlines represent the density of states. Red and blue filled areas show the occupation of electronic states by spin-up and spin-down electrons, respectively. **c** Population evolution of the electrons in the up-CB, up-VB and dn-VB regions for the three systems.

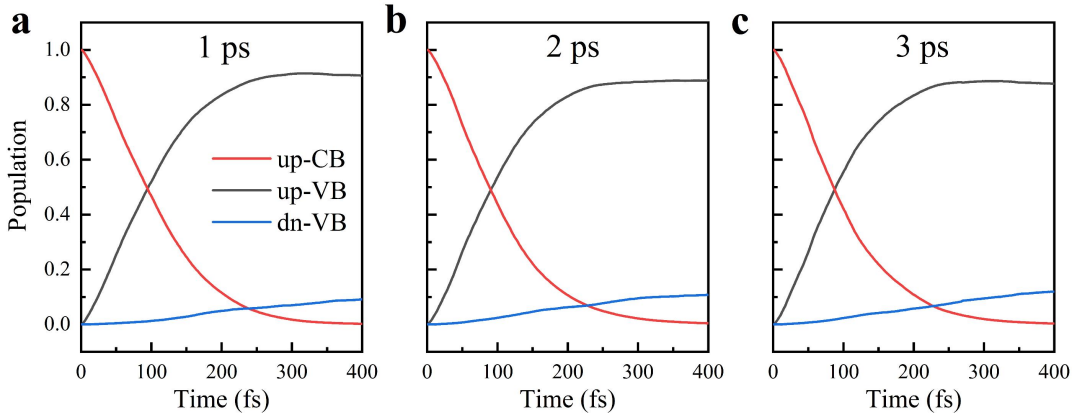

Supplementary Fig. S20 | Population evolution of electron in spin states in the pristine system. a-c AIMD for 1 ps, 2 ps and 3 ps, respectively.

References

1. Tully, J. C. Molecular dynamics with electronic transitions. *J. Chem. Phys.* **93**, 1061-1071 (1990).

2. Carig, C. F.; Duncan, W. R. & Prezhdo, O. V. Trajectory surface hopping in the time-dependent Kohn-Sham approach for electron-nuclear dynamics. *Phys. Rev. Lett.* **95**, 163001 (2005).

3. Granucci, G.; Persico, M. & Spighi, G. Surface hopping trajectory simulations with spin-orbit and dynamical couplings. *J. Chem. Phys*. **137**, 22A501 (2012).

4. Granucci, G. & Persico, M. Critical appraisal of the fewest switches algorithm for surface hopping. *J. Chem. Phys*. **126**, 134114 (2007).